DENTAL MATERIALS 35 (2019) e220–e233

Available online at www.sciencedirect.com

ScienceDirect

journal homepage: www.intl.elsevierhealth.com/journals/dema

Assessment of cytotoxicity and antibacterial effects of silver nanoparticle-doped titanium alloy surfaces

Yvoni Kirmanidou[a,1], *Margarita Sidira*[a,1], *Athina Bakopoulou*[a,*], *Alexandros Tsouknidas*[b], *Oleg Prymak*[c], *Rigini Papi*[d], *Theodora Choli-Papadopoulou*[d], *Matthias Epple*[c], *Nikolaos Michailidis*[b], *Petros Koidis*[a], *Konstantinos Michalakis*[a,*]

[a] *Department of Prosthodontics, School of Dentistry, Faculty of Health Sciences, Aristotle University of Thessaloniki (A.U.Th), Thessaloniki, Greece*

[b] *Department of Design and Structures, Physical Metallurgy Laboratory, School of Mechanical Engineering, Faculty of Engineering, Aristotle University of Thessaloniki (A.U.Th), Greece*

[c] *Inorganic Chemistry and Center for Nanointegration Duisburg-Essen (CeNIDE), University of Duisburg-Essen, Essen, Germany*

[d] *Department of Biochemistry, School of Chemistry, Faculty of Sciences, Aristotle University of Thessaloniki (A.U.Th), Thessaloniki, Greece*

ARTICLE INFO

Keywords:
Silver nanoparticles
Silver-doped titanium surfaces
Cytotoxicity
Antibacterial effects
Osteoblastic cells
Periopathogens

ABSTRACT

Objectives. This study aimed to develop silver nanoparticle (AgNP)-doped Ti_6Al_4V alloy surfaces and investigate their antibacterial properties against representative periopathogens and potential cytotoxicity on osteoblastic cells.

Methods. AgNPs of different size distributions (5 and 30 nm) were incorporated onto the Ti_6Al_4V surfaces by electrochemical deposition, using colloid silver dispersions with increasing AgNP concentrations (100, 200 and 300 ppm). The time-course silver release from the specimen surfaces to cell culture media was assessed by Atomic Absorption Spectroscopy (AAS). Cell attachment, viability and proliferation were investigated by SEM, live/dead staining MTT and BrdU assays. The antibacterial effects were assessed against *P. gingivalis* and *P. intermedia* by serial dilution spotting assays.

Results. A time- and concentration-dependent silver release from the experimental surfaces was observed. Overall, cell viability and attachment on the AgNP-doped surfaces, suggested adequate cytocompatibility at all concentrations. A transient cytotoxic effect was detected at 24 h for the 5 nm-sized groups that fully recovered at later time-points, while no cytotoxicity was observed for the 30 nm-sized groups. A statistically significant, concentration-dependent decrease in cell proliferation rates was induced at 48 h in all AgNP groups, followed by recovery at 72 h in the groups coated with 5 nm-sized AgNPs. A statistically significant, concentration-dependent antibacterial effect up to 30% was confirmed against both periopathogens.

* *Corresponding authors at*: Department of Prosthodontics, School of Dentistry, Faculty of Health Sciences, Aristotle University of Thessaloniki, GR-54124, Thessaloniki, Greece.

E-mail addresses: abakopoulou@dent.auth.gr (A. Bakopoulou), kmichalakis@dent.auth.gr (K. Michalakis).

https://doi.org/10.1016/j.dental.2019.06.003

Significance. This study sheds light to the optimal size-related concentrations of AgNP-doped Ti_6Al_4V surfaces to achieve antibacterial effects, without subsequent cytotoxicity. These results significantly contribute to the development of antibacterial surfaces for application in oral implantology.

1. Introduction

The wide application of commercially pure titanium and its alloys, such as Ti_6Al_4V for orthopedic and dental implants has brought them in the forefront of biomaterial science [1]. Their excellent biocompatibility, superior mechanical strength, high corrosion resistance and low modulus of elasticity lead to notable success and survival rates in both orthopedic (80–98.7%) and dental implants (90–96.5%) [2]. Despite their long-term survival rates, biological and mechanical complications are still reported [3,4].

Despite the adoption of aseptic surgical protocols supplemented by administration of antibiotic prophylaxis, implant-associated infections remain a challenging problem [5]. Efforts have been made for the development of antibacterial implant surfaces, aiming at prevention of bacterial attachment during the early phase of implantation or post-surgically [6]. Antibiotic-loaded surfaces have been reported in numerous in vitro studies, utilizing calcium phosphate, carbonated hydroxyapatite, biodegradable poly (lactic-*co*-glycolic acid) and polymeric nanoparticles as carriers and delivery agents [7]. Nevertheless, the presence of antibiotic-resistant pathogens has limited the incorporation of antibiotics into implant surface coatings, leading to the increasing use of inorganic nanoparticles like silver [8].

Silver has been a well-known antimicrobial agent since antiquity [9]. Engineering silver down to the nano-scale provides nanoparticles (AgNPs) sized up to 100 nm, which are more active than the bulk material due to their high surface to volume ratio. The antimicrobial activity of AgNPs has been demonstrated towards several viruses, fungi and a broad spectrum of bacteria strains, including *E. coli*, *S. aureus*, *K. pneumoninae*, *S. epidermidis*, *S. pyogenes*, *P. aeruginosa* and *S. mutans* [10–12]. Furthermore, oral anaerobic periopathogenic bacteria, such as *A. actinomycetemcomitans*, *F. nucleatum*, *P. gingivalis* and *P. intermedia,* have been also reported to be prone to the antibacterial action of AgNPs [13]. This effect seems to be concentration- and time-dependent but also related to the size, shape and capping agents (i.e. organometallic precursors coating the nanoparticles, acting as stabilizing agents by preventing nanoparticle aggregation and overgrowth) of the nanoparticles [14].

The excellent antibacterial properties of AgNPs have led to the development of AgNP-coated titanium surfaces via numerous methods of deposition, including ion implantation, physical vapor deposition (PVD), plasma electrolytic oxidation (PEO) and chemical reduction [15]. Among them, electrophoretic deposition is an easy, cost-effective and highly productive technique that provides the ability to create thin, nanostructured surfaces [16].

However, the incorporation of AgNPs on titanium implant surfaces has been also a "double-edged sword", because of the strong cytotoxic effects of silver on several types of eukaryotic cells [17]. As a result, concerns have been raised, regarding the possible deleterious effects of nanostructured silver on human health and environmental safety [18]. According to Xiu et al. the toxicity of AgNPs is attributed to the Ag^+ ion release, that is influenced by the oxygen interaction, the NP size, shape, as well as the coating [19]. The potential mechanisms of silver toxicity that have been described so far include induction of oxidative stress [20], "Trojan-horse effect" [21] (i.e. a phenomenon of bioconcentration in which the incorporation of nanoparticles intracellularly can lead to further release of silver ions), mitochondrial dysfunction and DNA damage [22].

Regarding the impact of AgNPs on primary osteoblasts and osteoblastic cell lines, the results described in the literature are quite controversial [23]. Shen et al. reported decreased cytotoxicity of a chromium-cobalt alloy after the incorporation of AgNPs, as compared to control [9]. While Zheng et al. reported increased proliferation of primary rat osteoblasts cultured on titanium surfaces after hydrothermal treatment with H_2O_2, followed by Ag plasma immersion ion implantation [13]. Similarly, Kaczmarek et al. indicated high biocompatibility of AgNP-deposited anodized titanium surfaces, evaluated on human osteosarcoma cell-line cultures [24]. Nevertheless, most of the studies suggest that the cytotoxic activity of AgNPs occurs at a higher concentration range for the eukaryotic cells than for the prokaryotic bacteria, indicating that an optimal "therapeutic window" must be determined to enable successful application of AgNP-doped titanium surfaces in the biomedical field [10,25].

Based on the above, it was the aim of the present study to evaluate the effects of electrophoretically prepared AgNP-doped Ti_6Al_4V surfaces, using AgNP colloid dispersions of two different size distributions (monodispersed around 5 nm and 30 nm respectively) and increasing AgNP concentrations (100, 200 and 300 ppm) on the metabolic activity and proliferation rates of human osteoblastic cells, as well as their antibacterial effects on two representative anaerobic oral periopathogenic bacteria, *P. gingivalis* and *P. intermedia*. The research (null) hypothesis was that the size and concentration of the AgNPs have no impact on the above-mentioned biological endpoints of the eukaryotic and prokaryotic cells.

[1] These authors contributed equally to this work.

2. Materials and methods

2.1. Preparation and characterization of AgNP-doped Ti_6Al_4V surfaces

2.1.1. Titanium alloy specimen preparation and electrochemical deposition of AgNPs

Ti_6Al_4V machined discs with a diameter of 6 mm and a height of 1 mm were kindly provided by ADIN (ADIN Dental Implant Systems, Avula, Israel). The specimens were ultrasonically cleaned (Bandelin Sonorex, Berlin) in an 100% ethanol solution for 20 min prior to silver deposition. For the electrochemical deposition, the specimens were immersed in colloid silver solutions (PLiN Nanotechnology S.A., Thessaloniki, Greece) with positively charged AgNPs of size distributions of 5 and 30 nm (Fig. 1a,b), as determined by Dynamic Light Scattering (DLS) and concentrations of 100, 200 and 300 ppm. A direct current of 20 Volt (V) was supplied for approximately 5 min (min), using the specimens as the cathode and a commercially pure titanium plate (Grade 2) as the anode. To maintain a standard distance of 6 mm between the anode and the cathode, poly-lactic acid (PLA) moulds were fabricated. The moulds were designed in a CAD software (3D CAD, Solidworks, Massachusetts, U.S.A.) and 3-dimensionally printed using the open-source FDM (Fused Filament Fabrication — FFF) printer (Mendelmax 2.0). As a result, six experimental groups and one control group were included in this study based on the AgNP size and concentration of the initial colloid solution: (1) control (Ti_6Al_4V), (2) 5 nm/100 ppm, (3) 5 nm/200 ppm, (4) 5 nm/300 ppm, (5) 30 nm/100 ppm, (6) 30 nm/200 ppm, (7) 30 nm/300 ppm. After electrodeposition, all specimens were ultrasonically cleaned in ethanol for 20 min, rinsed thoroughly in distilled water and dried in an ambient environment. For all further experimental assays, the discs were sterilized under UV irradiation for 30 min.

2.1.2. Surface characterization of the samples by scanning electron microscopy and energy dispersive X-ray spectroscopy (SEM-EDX)

To evaluate the surface topography and analyze the chemical composition of the specimens, SEM examination was performed with an ESEM Quanta 400 FEG instrument (FEI), equipped with EDX spectroscopy (EDX; Genesis 4000, SUTW-Si (Li) detector) operating in a high vacuum with gold/palladium-sputtered samples with an average thickness of 2 nm. For the sputtering a c̈ressington sputter coater 108 autoḋevice was used. All SEM analyses were performed with a 5 kV accelerating voltage and 0.4 mA probe. For EDX analysis a 15 kV accelerating voltage was used. The images were taken in magnifications of ×10,000–100,000.

2.1.3. Investigation of silver release from the AgNP-doped Ti_6Al_4V surfaces using atomic adsorption spectroscopy (AAS)

For the determination of the amount of the released silver in biological media, AAS was employed. The biological medium that was used was an a-Modification of Eagle's Medium (a-MEM), supplemented with 10% Fetal Bovine Serum (FBS), 100 mM L-ascorbic acid phosphate, 100 units/ml penicillin, 100 mg/ml streptomycin and 0.25 mg/ml Amphotericin B (all from Invitrogen, Karlsruhe, Germany) (=Complete Culture Medium — CCM) and was the same medium used for the in vitro assays of this study, as described in Section 2.2.1.

The specimens of each experimental group were placed inside the wells of 48-well plates. Cells were seeded on the top of the specimens at 104 cells/specimen (as described in 2.2) and incubated in 500 μl of CCM for either 24, 48 or 72 h at 37 °C and 5% CO_2. At each time-point, the culture supernatant was collected and processed for AAS analysis. AAS was carried out on a ThermoElectron M-Series spectrometer with a graphite tube furnace according to DIN EN ISO/IEC 17025:2005.

2.2. Cytotoxicity assessment of the AgNP-doped Ti_6Al_4V surfaces

2.2.1. Cell culture

SaOS-2 osteoblast-like cell lines, obtained from the American Type Culture Collection (ATCC No. HTB 85) were expanded in CCM in 75 cm^2 flasks. Cell cultures were maintained in an incubator at 37 °C, in 5% CO_2 and 95% humidity until reaching 80–90% confluency. Cell harvesting from the flask surface was performed using 0.25% Trypsin/1 mM EDTA solution (Invitrogen). Finally, for cell counting and determination of cell density and percentage of dead cells before each experimental assay, an improved Neubauer hemocytometer (Laboroptik, Lancing, UK) and Trypan Blue exclusion tests were employed.

2.2.2. Evaluation of the cell attachment and morphology by SEM

The attachment properties and morphology of the cells after 72 h of direct contact with the experimental surfaces were evaluated by means of SEM. In brief, cell-seeded specimens were washed with PBS, fixed with 3% glutaraldehyde in 0.1 M sodium cacodylate buffer (pH = 7.4), and dehydrated in a graded series of ethanol concentrations (35, 50, 70, 95 and 100%). Finally, specimens were dried in a critical point drier (Baltec CPD 030), sputter-coated with a 20 nm thick layer of gold-palladium (Baltec SCD 050) and observed under a SEM (JEOL JSM-6390 LV) at an accelerating voltage of 15–20 kV.

2.2.3. Evaluation of cell viability by live/dead fluorescence staining

For the live/dead assay, the specimens of each experimental group were placed inside the wells of 48-well plates. Cells were seeded on the top of the specimens at 10^4 cells/specimen and incubated in CCM for 24 and 72 h at 37 °C. At each time-point, cells were double stained with Calcein AM (live) and Ethidium Homodimer-EthD1 (dead) fluorescent stains and observed under a confocal microscope (Leica Microsystems, Wetzlar, Germany). Approximately 5–10 serial sections were obtained, and the z-stacked images produced.

2.2.4. Evaluation of cell viability by the MTT assay

The viability of Saos-2 cells seeded on the top of the experimental specimens of each group was investigated by the MTT [3-(4,5-dimethylthiazol-2-yl)-2,5-diphenyltetrazolium bromide] assay. Cells were cultured in direct contact with the specimens in 48-well plates (104 cells/well) for 24, 48 and 72 h, at 37 °C and 5% CO_2. After these three time-points, MTT

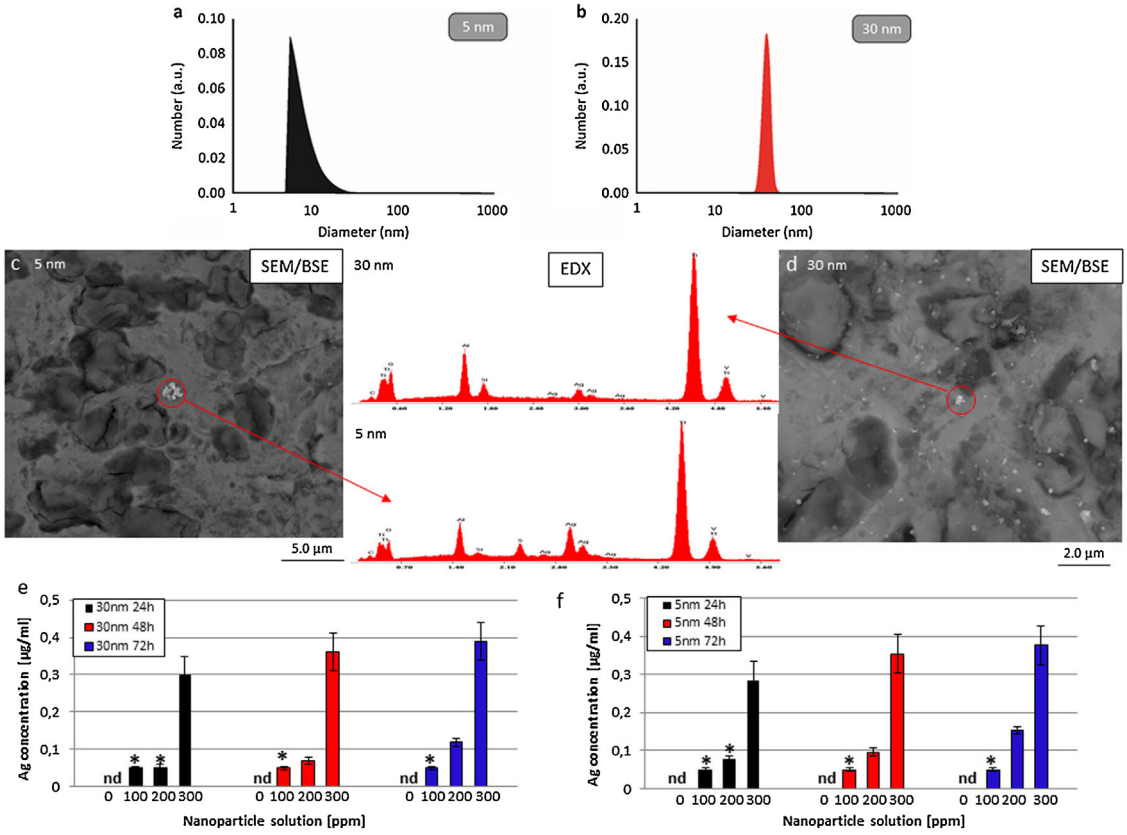

Fig. 1 – (a, b) Size distribution profiles of nanoparticle dispersions, determined by Dynamic Light Scattering based on an iterative algorithm (SBL): (a) for the 5 nm solution and (b) for the 30 nm solution respectively (c, d) SEM/BSE (back scattered electron mode) microphotographs of AgNano aggregates on the Ti6Al4V surfaces, doped with: (c) 5 nm- and (d) 30 nm-sized AgNPs at a concentration of 300 ppm showing their presence as "white spots" (red cycles) and the respective EDX patterns, confirming the existence of silver. (e, f) Results of the AAS analysis of Ti_6Al_4V specimens coated with (e) 5 nm - and (f) 30 nm-sized AgNPs using colloid dispersions with increasing AgNP concentrations of 0, 100, 200 and 300 ppm after 24, 48, 72 h of incubation in culture medium. Results are indicative of a time- and concentration-dependent release of silver (n.d: not detectable, *: value <0.05 µg/ml, which is the detection limit of the AAS device).

(5 mg/ml in CCM) was added in each well containing the specimens and the plates were incubated for 4 h at 37 °C and 5% CO_2. During this period, the NAD(P)H-dependent cellular oxidoreductase enzymes of mitochondria reduce the tetrazolium dye MTT to its insoluble, which has a purple color. After this period, the medium containing the MTT solution was discarded and 500 µl of DMSO (Dimethyl sulfoxide) were added in each well and incubated for 1 h at 37 °C to dissolve the insoluble purple formazan product into a colored solution. Then, the specimens were removed from the wells and the optical density (OD) was measured against blank (DMSO) at a wavelength of 545 nm and a reference filter of 630 nm by a microplate reader (Epock, Biotek, Biotekree times, with 6–8 replicates for each repetition were repeated three times, with 6–8 replicates for each repetition. All results were expressed as an average % percentage of the control value (cells seeded on uncoated Ti_6Al_4V specimens).

2.2.5. *Evaluation of cell proliferation by the BrdU assay*

The proliferation rate of Saos-2 cells seeded on the top of the experimental specimens of each group was investigated by the BrdU (5-bromo-2′-deoxyuridine) assay (Sigma–Aldrich, Roche Diagnostics, Manheim, Germany). Cells were cultured in direct contact with the specimens in 48-well plates (104 cells/well) for 24, 48 and 72 h, at 37 °C and 5% CO_2, as described in 2.2.4 for the MTT assay. After these three time-points, BrdU was added at a concentration of 10 µM and the plates incubated for 6 h at 37 °C and 5% CO_2. Then, treated cells were fixed with FixDenat® solution (at 15–25 °C, for 30 min), according to the manufacturer's recommendations and exposed to a peroxidase-conjugated BrdU antibody (anti-BrdU-POD) at a concentration of 10 µM for 90 min. Afterwards, 200 µl of 3-3′-5-5′-tetra-methyl-benzidine substrate (TMB) were added in each well. The blue color peroxidase-substrate reaction was ended after 5 min, by an H2SO4 solution (stop solution, 50 µl/well). The incorporated BrdU was quantified by measuring the OD in a microplate reader (Epock, Biotek, Biotek Instruments, Inc., Vermont, U.S.A.) at a wavelength of 450 nm and a reference filter of 690 nm. Cell-free and BrdU-free wells served as internal controls for this assay. The resulting OD values of those wells were used as blank (negative control) and background control (positive control), respectively. The experiments were

repeated three times, with 6–8 replicates for each repetition. All results were expressed as an average % percentage of the control value (cells seeded on uncoated Ti_6Al_4V specimens).

2.3. Antibacterial effects of the AgNP-doped Ti_6Al_4V surfaces

2.3.1. Evaluation of the antibacterial effects against P. gingivalis and P. intermedia

The antibacterial effects of the experimental surfaces were examined using the Serial Dilution Spotting Assay (SDSA, ISO 20743:2007). Both *P. gingivalis* (DSM 20709) and *P. intermedia* (DSM 20706) bacteria strains were obtained by the Leibniz-Institut DSMZ (Leibniz-Institut, Deutsche Sammlung von Mikroorganismen und Zellkulturen GmbH, Braunschweig, Germany). Bacterial cultures were anaerobically expanded in BHI-broth (Difco Laboratories, Detroit, USA) with 1 mg/ml vitamin K and 5 mg/ml heme (Bacteria Culture Medium — BCM), as previously described [26]. Anaerobic conditions were developed (80% N_2, 10% H_2, 10% CO_2) using the GasPak EZ Gas Generating Pouch Systems (BD, Benex Limited, Dublin, Ireland). In brief, both bacterial pre-cultures were initially grown in 5 ml BHI-broth, at 150 rpm and 37 °C, in anaerobic environment. Following, 50 ml BHI-broth solutions were inoculated with 4–5 % v/v of the initial pre-cultures. The resulting cultures were further expanded under the same conditions until reaching an optical density of 0.6–0.7, measured at 600 nm by an ELISA plate reader.

Afterwards, the expanded cultures were poured into to 48 well plates (0.5 ml/well) and anaerobically incubated in direct contact with the specimens, at 37 °C and 50 rpm for 24 h. Live bacterial cells were harvested from the test surfaces, using 2.0 ml (4 × 0.5 ml) TAT solution (Enzymatic Digest of Casein 20 g/l, Polysorbate 20 40 ml/l, Lecithin 5 g/l). Each initial inoculum was resuspended in serial ten-fold dilutions of BHI-broth. Aliquots of 0.1 ml of each dilution were spot-plated on solid agar (Anaerobe CDC Blood Agar, Bioprepare, Warrington, United Kingdom). The cultures were incubated at 37 °C in anaerobic conditions for 72 h. Finally, Colony Forming Units (CFU) were counted and % reduction was determined by the following equation: $\%\ \text{reduction} = (CFU_{control} - CFU_{test}) \times 100/CFU_{control.}$ All experiments were performed in triplicates, three times for each bacteria strain.

2.3.2. Evaluation of the bacterial morphology by SEM

Evaluation of the morphological characteristics of the bacterial cells in direct contact with the experimental surfaces was performed by means of SEM at 24 h after seeding. The procedures followed for sample preparation were like those described for the eukaryotic cells in 2.2.2. SEM examination was performed with an ESEM Quanta 400 FEG instrument (FEI).

2.4. Statistical analysis

For the statistical analysis the Prism 6 (GraphPad, CA, U.S.A.) software was utilized. Two-way ANOVA analysis was performed for all viability and antibacterial assays, while for follow-up comparisons between groups and time-points the Tukey's post-hoc test was employed. Normal distribution was confirmed by Kolmogorov–Smirnov normality tests. The level of statistical significance was set to 0.05 ($p < 0.05$)

3. Results

3.1. Characterization and silver release from AgNP-doped Ti6Al4V surfaces

Even though monodispersed AgNPs could not be observed (due to the SEM resolution), EDX analyses confirmed the presence of Ag on the surfaces in the form of "white spots", randomly distributed within the SEM microphotographs.

AAS analysis revealed a time- and concentration-dependent release of silver from all experimental groups (Fig. 1e,f). Specimens of 300 ppm presented the highest values of silver release at both AgNP sizes: 5 nm [0.28, 0.35, 0.37 μg/ml] and 30 nm [0.3, 0.36, 0.39 μg/ml] after 24, 48 and 72 h respectively. The reported values for specimens of 200 ppm were: 5 nm [0.07, 0.09 and 0.15 μg/ml] and 30 nm [0.05, 0.06 and 0.11 μg/ml] after 24, 48 and 72 h respectively. Specimens of the 5 nm/100 ppm and 30 nm/100 ppm experimental groups presented minimal silver release, that was at the range of the detection limit of the AAS device (0.05 μg/ml), as indicated by asterisks in the respective bars in Fig. 1(e, f). Uncoated (control, Ti_6Al_4V specimens) showed no silver release (non-detected; nd)

3.2. Cytotoxicity assessment of AgNP-doped Ti_6Al_4V surfaces

3.2.1. Evaluation of cell attachment and morphology by SEM

SEM microphotographs of SaoS-2 cells in direct contact with the specimens of each group at 72 h after cell seeding revealed that a typical confluent cell layer could be formed on all types of experimental surfaces. The cells appeared to be intimately attached to all surfaces and were evenly spread throughout the coated area, even in close contact with the silver spots. SaOS-2 exhibited a typical polygonal shape and several cytoplasmic extensions and filopodia, that seemed not to be affected by increasing concentrations of the AgNP-coating solution (Fig. 2a–p)

3.2.2. Evaluation of cell viability by live/dead staining

Cell viability was initially evaluated by live/dead fluorescent staining and visualization by confocal microscopy. As shown in the z-stacked images (Fig. 3(a–p)), most cells appeared green, metabolizing the calcein AM fluorescent stain. This is an indication that they remained viable throughout the culture period up to 72 h. In contrast, very few dead cells were observed as red rounded bodies incorporating the ethidium homodimer DNA intercalating dye. Moreover, it was observed that the cells were uniformly distributed and attached on the surfaces of all specimens indicating the effective colonization, survival and proliferation over time of SaOS-2 on the surfaces of all experimental groups (Fig. 3a–p)

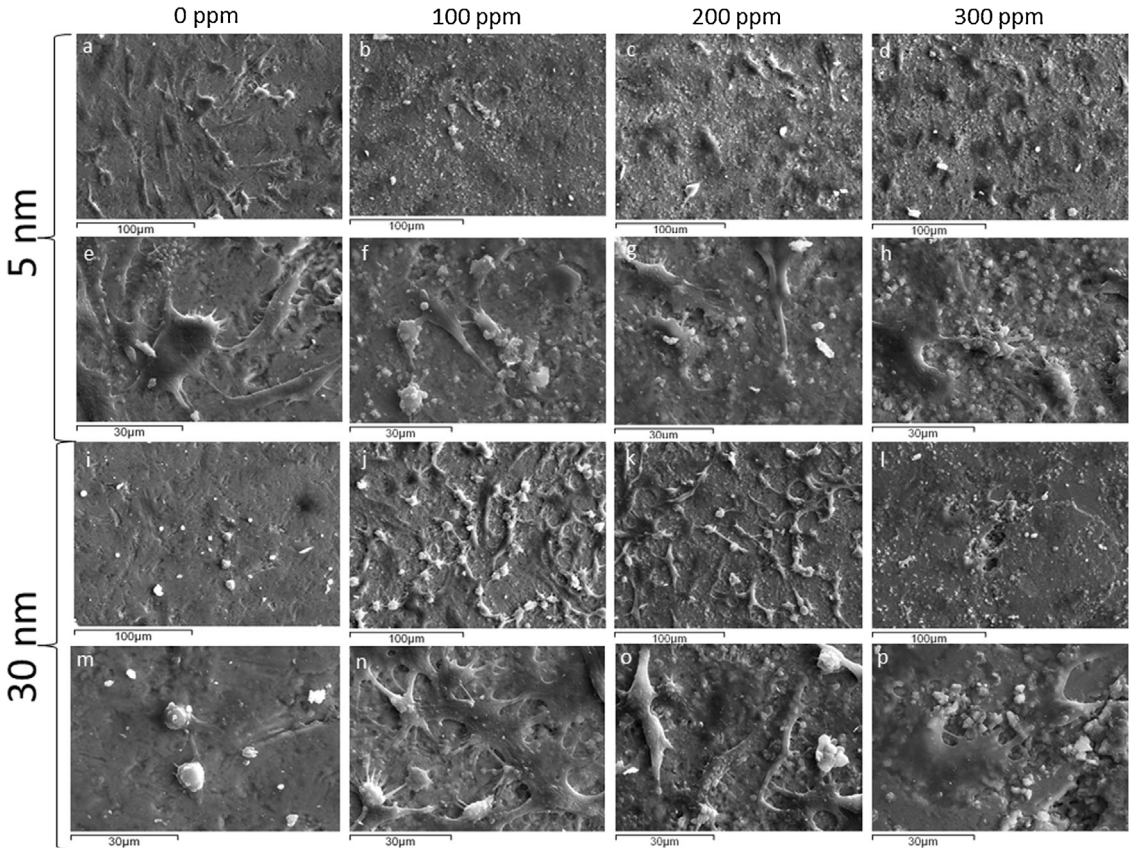

Fig. 2 – (a–p) SEM microphotographs of Ti_6Al_4V specimens coated with 5 nm- and 30 nm-sized AgNPs at concentrations of 0, 100, 200 and 300 ppm, indicating proper attachment and spreading of SaOS-2 osteoblastic cells on all experimental titanium surfaces 72 h after cell seeding.

3.2.3. *Evaluation of cell viability by the MTT assay*

Cell viability was further evaluated by the MTT metabolic-based test. Overall, a time- and concentration-dependent ($p < 0.05$) change of cell metabolic activity was observed for both 5- and 30 nm AgNP-doped surfaces, but with differential time-course patterns, as depicted in Fig. 4(a,b).

In specific, the 5 nm AgNP-doped surfaces showed a decreased cell metabolic activity at 24 h in all concentration groups (100, 200 and 300 ppm), as compared to the uncoated titanium surfaces (control, Ti_6Al_4V). This activity recovered, showing a statistically significant higher value compared to the control for the 5 nm/100 ppm group at 48 and 72 h ($p < 0.05$ and $p < 0.01$ respectively) and for the 5 nm/200 ppm group at 72 h ($p < 0.01$). In contrast, the 5 nm/300 ppm group showed no statistically significant increase in cell metabolic activity at 48 and 72 h compared to the control group (Ti_6Al_4V).

For the 30 nm AgNP-coated surfaces, it was shown that no reduction of cell metabolic activity compared to the control group (Ti_6Al_4V) could be observed at 24 h. Similarly to the 5 nm-groups of the same concentrations, the 30 nm/100 ppm- and 30 nm/200 ppm groups exhibited a statistically significant increase in cell metabolic activity at 48 h ($p < 0.05$ for both groups) compared to the control group (Ti_6Al_4V), while no such increase could be detected for the 30 nm/300 ppm group at neither time-point (48 or 72 h).

The results of the MTT cell viability assay overall indicate an initial (at 24 h) cytotoxic effect for the 5 nm AgNP-coated surfaces, that fully recovered at later time-points and absence of cytotoxicity of all 30 nm AgNP-coated groups.

3.2.4. *Evaluation of cell proliferation by the BrdU assay*

Cytotoxicity assessment of the AgNP-doped surfaces on SaOS-2 cells was further performed using another biological endpoint, i.e. the impact on cell proliferation rate by means of the BrdU assay. Overall, a time- and concentration-dependent ($p < 0.05$) change of cell proliferation rate was observed for both 5- and 30-nm AgNP-doped surfaces, but with differential time-course patterns, as depicted in Fig. 5(a,b).

In specific, in the group of 5 nm sized AgNP-doped surfaces, the only statistically significant decrease of cell proliferation compared to control (Ti_6Al_4V) was that of the 5 nm/300 ppm group at 48 h ($p < 0.001$), while no significant differences were observed for the other groups and time-points. At the same time-point of 48 h, statistically significant differences could be observed among the different AgNP concentrations, i.e. 5 nm/300 ppm <5 nm/200 ppm <5 nm/100 ppm ($p < 0.01$). Interestingly, this relationship was reversed at 72 h, as there was an increase in cell proliferation rate for the 5 nm/200 ppm and 5 nm/300 ppm reaching levels not statistically significant to control ($ps > 0.05$). In this respect, the final concentration relationship was: 5 nm/100 ppm < 5 nm/200 ppm = 5 nm/300 ppm.

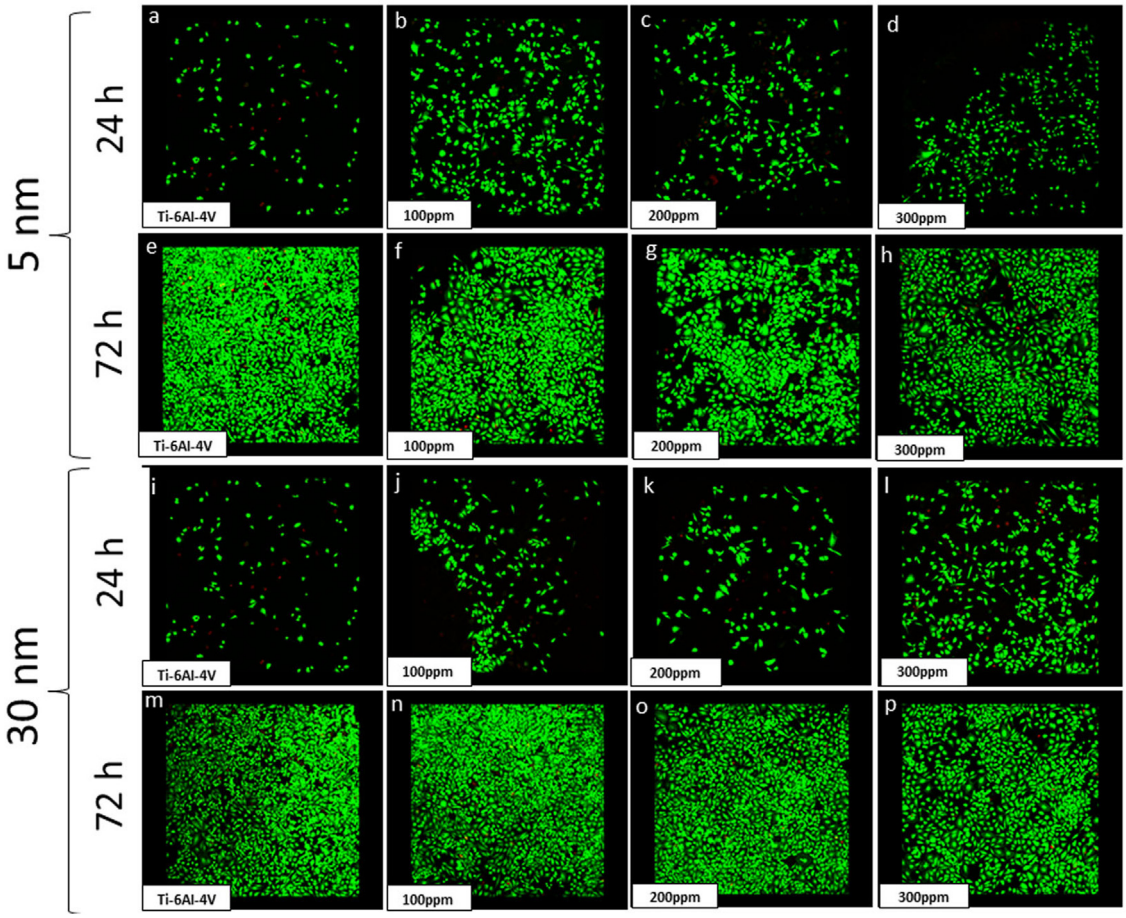

Fig. 3 – (a–p) Confocal microscopy microphotographs (live/dead fluorescent staining with Calcein AM and EthD-1) showing high levels of cell viability of SaOS-2 osteoblastic cells on all the AgNP-doped Ti_6Al_4V surfaces of both size groups of 5 nm and 30 nm after 24 and 72 h of incubation.

For the 30 nm AgNP-doped surfaces, a similar trend compared to the 5 nm experimental groups was observed at 48 h, with statistically significant reduction of cell proliferation compared to control (Ti6Al4V) only for the 30 nm/300 ppm group ($p < 0.01$) and a similar relationship between different concentrations, i.e. 30 nm/300 ppm < 30 nm/200 ppm < 30 nm/100 ppm ($p < 0.01$). In contrast to the 5 nm sized AgNPs experimental groups, no recovery of cell proliferation rate could be observed in the test group of 300 ppm/30 nm at 72 h, as cell proliferation remained significantly lower compared to control (Ti_6Al_4V, $p < 0.01$).

The results of the BrdU celsl proliferation assay overall indicate a cytotoxic effect of both the 5- and 30 nm sized AgNP-coated surfaces at 48 h, that fully recovered at 72 h for the 5 nm- but not for the 30 nm-sized experimental groups.

3.3. *Antibacterial effects of the AgNP-doped Ti_6Al_4V surfaces*

3.3.1. *SEM evaluation of bacterial colonies on the AgNP-doped Ti_6Al_4V surfaces*

SEM microphotographs of bacterial colonies on the experimental surfaces after 24 h of incubation indicate a concentration-dependent decrease of both bacterial cells *P. gingivalis* (Fig. 6A(a–d)) and *P. intermedia* (Fig. 6B (a–d)). The numbers of both cells were substantially decreased in the 5 nm/300 ppm- and the 30 nm/300 ppm groups, as compared to the 5 nm/100 ppm and the s30 nm/100 ppm groups respectively. The latter showed a profile of more separated and undamaged bacterial cells, while, in contrast, cell debris, lysed bacteria with disrupted cell surfaces and numerous craters could be observed on the 5 nm/300 ppm and 30 nm/300 ppm specimens.

3.3.2. *Evaluation of the reduction of bacterial colony forming ability on the AgNP-doped Ti_6Al_4V surfaces*

The decrease in number of viable bacterial colonies was further confirmed by the results of the SDSA assay. There was a concentration-dependent % reduction of colony forming units (CFUs) of *P. gingivalis* in direct contact with all experimental groups, as compared to control (Fig. 6A e). The difference reached statistical significance in both 5 nm/200 ppm and 30 nm/200 ppm groups ($p < 0.001$). The maximum reduction percentages were $29.9 \pm 3.5\%$ and $26 \pm 4.1\%$, for the 5 nm/300 ppm and 30 nm/300 ppm groups respectively ($p < 0.001$).

The results related to *P. intermedia* were similar to those obtained for the *P. gingivalis* (Fig. 6B e). The differences

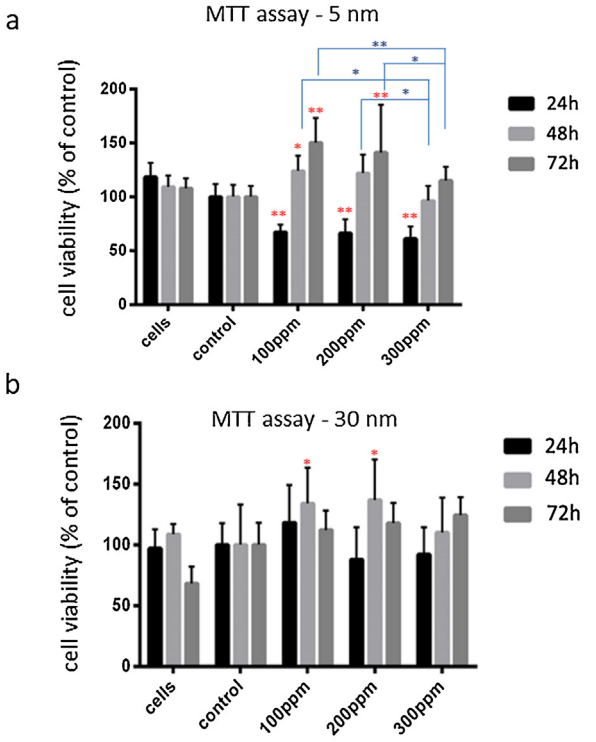

Fig. 4 – (a, b) Evaluation of metabolic activity of SaOS-2 osteoblastic cells seeded on the AgNP-doped Ti_6Al_4V surfaces of (a) 5 nm and (b) 30 nm after 24, 48 and 72 h, as assessed by the MTT assay. The optical density (OD) was measured against blank (DMSO) at 545 nm with a reference filter at 630 nm. The red asterisks indicate statistically significant differences between CONTROL (Ti_6Al_4V) and each of the 100 ppm-, 200 ppm- or 300 ppm groups for the same time-point (24 or 48 or 72 h) and the same AgNP size (5 nm or 30 nm). Blue brackets indicate statistically significant differences between 100 ppm vs. 200 ppm, 200 ppm vs. 300 ppm and 100 ppm vs. 300 ppm for the same time-point (24 or 48 or 72 h) and the same size (5 nm or 30 nm) ($^*p < 0.05$ and $^{**}p < 0.01$).

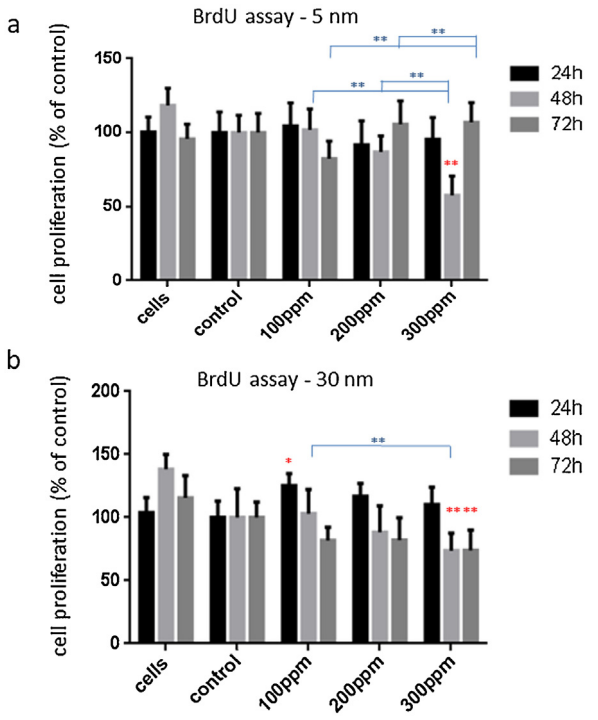

Fig. 5 – (a, b) Evaluation of cell proliferation of SaOS-2 osteoblastic cells seeded on the AgNP-doped Ti_6Al_4V surfaces of (a) 5 nm and (b) 30 nm after 24, 48 and 72 h, as assessed by the BrdU assay. The optical density (OD) was measured against blank (cell-free and BrdU-free wells) at 450 nm with a reference filter at 690 nm. The red asterisks indicate statistically significant differences between CONTROL (Ti_6Al_4V) and each of the 100 ppm-, 200 ppm- or 300 ppm groups for the same time-point (24 or 48 or 72 h) and the same AgNP size (5 nm or 30 nm). Blue brackets indicate statistically significant differences between 100 ppm vs. 200 ppm, 200 ppm vs. 300 ppm and 100 ppm vs. 300 ppm for the same time-point (24 or 48 or 72 h) and the same size (5 nm or 30 nm) ($^*p < 0.05$ and $^{**}p < 0.01$).

reached statistical significance compared to control for the 5 nm/200 ppm and 30 nm/200 ppm ($p < 0.01$) groups, showing the maximum reduction of CFUs at 5 nm/300 ppm and 30 nm/300 ppm (29.5 ± 4.2% and 26.11 ± 10.7%, respectively, $p < 0.01$).

4. Discussion

The objective of this study was to develop and characterize novel antibacterial AgNP-doped titanium alloy surfaces for potential applications in oral implantology. To the authors' knowledge this is the first study related to AgNP-doped titanium alloy surfaces, in which different nanoparticle sizes and concentrations were assessed regarding their biocompatibility, as well as antibacterial effects against two major periopathogens. Additionally, the present study sheds light on the effect of time- and concentration-dependent silver release from the developed AgNP-doped surfaces on both the metabolic activity and proliferation rates of human osteoblast cell-lines.

In the present study, three different AgNP solution concentrations and two AgNP sizes were used for electrochemical deposition of the titanium alloy surfaces, aiming to determine a "therapeutic window" between antibacterial activity and lack of cytotoxicity. The recommended by the manufacturer AgNP solution concentration (300 ppm) was applied, in addition to serial dilutions of the stock solution, to further evaluate whether even lower concentrations (100 and 200 ppm) could produce surfaces with effective antibacterial activity, while reducing potential cytotoxic effects to the eukaryotic cells. Based on the results of this study, the recommended concentration was found to be the most effective, without causing major cytotoxic effects. Regarding the AgNP sizes, 5 and 30 nm were selected based on existing literature data. According to previous studies [21], the smaller nanoparticles are internalized faster into the cells with a range of optimum radii of 25–50 nm showing the lowest rapping times. For this reason,

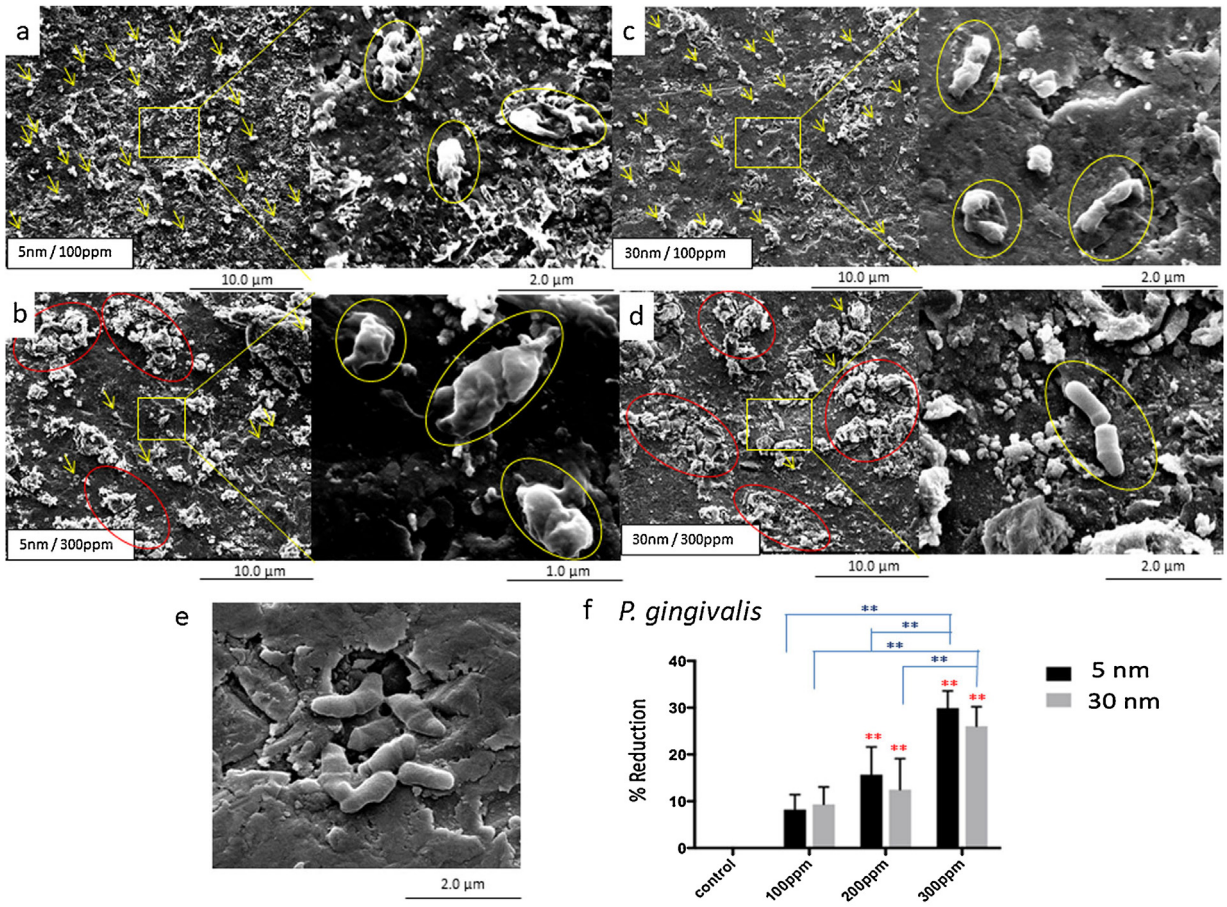

Fig. 6 – (A) (a–d) SEM microphotographs of Ti_6Al_4V specimens coated with (a) 5 nm-sized AgNPs at 100 ppm, (b) 5 nm-sized AgNPs at 300 ppm, (c) 30 nm-sized AgNPs at 100 ppm and (d) 30 nm-sized AgNPs at 300 ppm after 24 h of incubation with anaerobic cultures of the periopathogenic bacterium *P. gingivalis*. The yellow arrows and the yellow cycles indicate the presence of separated and undamaged bacterial cells. The red cycles indicate the presence of cell debris with disrupted bacterial surfaces. (e) Growth reduction of *P. gingivalis* after 24 h of direct contact with the AgNP-doped Ti_6Al_4V surfaces of 5 nm and 30 nm, showing a concentration-dependent % reduction of the bacterial colony forming units (CFUs). The red asterisks indicate statistically significant differences between CONTROL (Ti_6Al_4V) and each of the 100 ppm-, 200 ppm- or 300 ppm groups Blue brackets indicate statistically significant differences between 100 ppm vs. 200 ppm, 200 ppm vs. 300 ppm and 100 ppm vs. 300 ppm for the same size (5 nm or 30 nm). ($^*p < 0.05$ and $^{**}p < 0.01$). (B) (a–d) SEM microphotographs of Ti_6Al_4V specimens coated with (a) 5 nm-sized AgNPs at 100 ppm, (b) 5 nm-sized AgNPs at 300 ppm, (c) 30 nm-sized AgNPs at 100 ppm and (d) 30 nm-sized AgNPs at 300 ppm after 24 h of incubation with anaerobic cultures of the periopathogenic bacterium *P. intermedia*. The yellow arrows and the yellow cycles indicate the presence of separated and undamaged bacterial cells. The red cycles indicate the presence of cell debris with disrupted bacterial surfaces. (e) Growth reduction of *P. intermedia* after 24 h of direct contact with the AgNP-doped Ti_6Al_4V surfaces of 5 nm and 30 nm, showing a concentration-dependent % reduction of the bacterial colony forming units (CFUs). The red asterisks indicate statistically significant differences between CONTROL (Ti_6Al_4V) and each of the 100 ppm-, 200 ppm- or 300 ppm groups Blue brackets indicate statistically significant differences between 100 ppm vs. 200 ppm, 200 ppm vs. 300 ppm and 100 ppm vs. 300 ppm for the same size (5 nm or 30 nm). ($^*p < 0.05$ and $^{**}p < 0.01$).

the size of 30 nm was selected as being within the optimal range. On the other hand, based on another study [27], smaller AgNPs (~10 nm) are more active, due to their enhanced silver ion release from their increased total surface. According to the above study, the enhanced silver release leads to higher cytotoxicity to eukaryotic cells. Thus, the aim of our study was to compare the above-mentioned sizes (5 and 30 nm) regarding the optimum antibacterial, but not cytotoxic to eukaryotic cells, effects. Electrophoretic deposition was employed because it is a simple, versatile, time and cost-efficient method [15,16]. The presence of evenly distributed aggregates rather than a homogenous silver coating, allows for a combination of the antibacterial properties of silver, while leaving a substantial surface to exert the high osseointegration potential of titanium alloys [2,3].

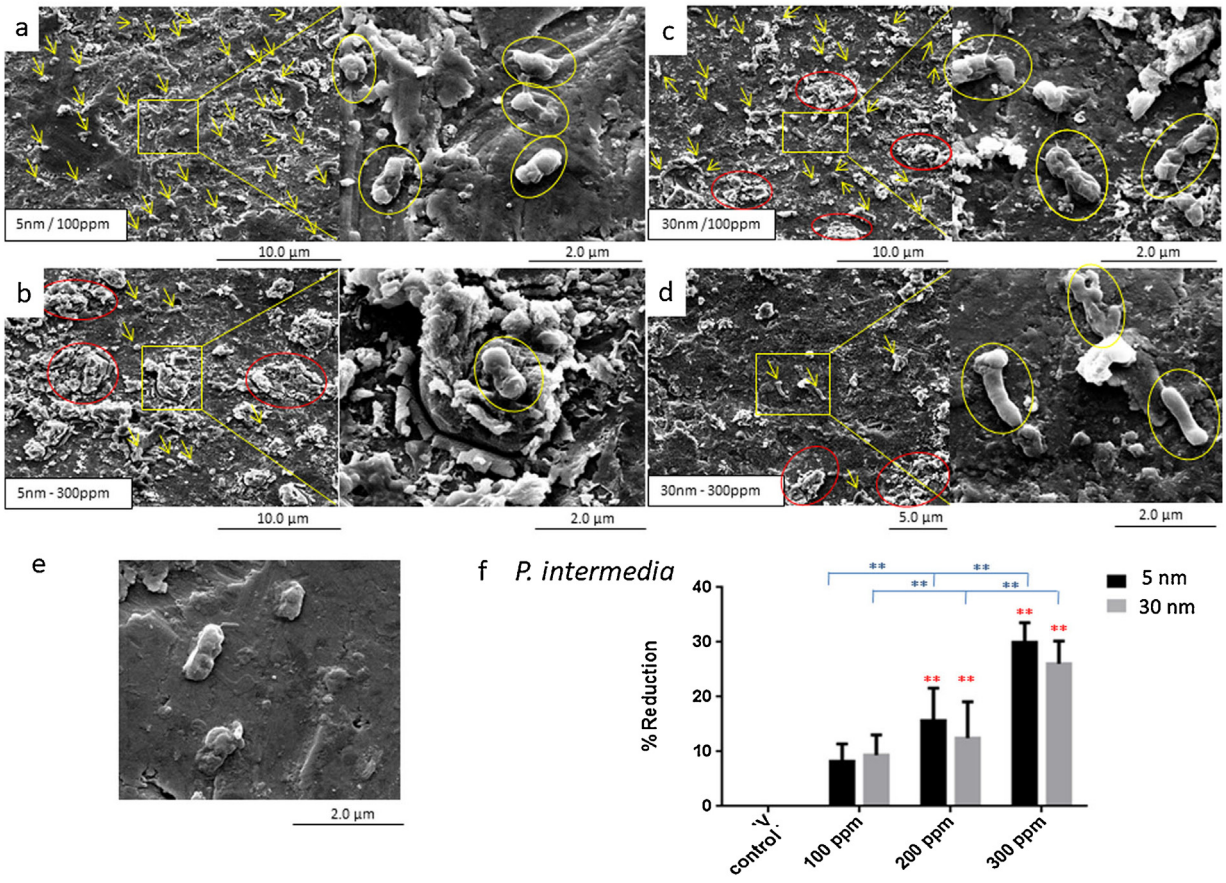

Fig. 6 – (*Continued*)

According to the AAS analysis, silver release in the culture medium was time- and concentration-dependent for both nanoparticle size distributions under investigation. Similarly, Zhang et al. reported higher silver ion release rates when the AgNP concentration increased from 300 μg/l to 600 μg/l. In addition to these findings, smaller particles presented higher silver release rates among different particle size distributions (20, 40 and 60 nm) [28]. Dobias and Latmani reported a significant increase in silver release (up to 85–89%) when the AgNP size decreased from 50 to 5 nm, during the same time frames [29]. This is attributed to the higher formation enthalpies (i.e. the net change associated with breaking the chemical bonds of the standard state elements and forming new bonds to create the compound of interest), as well as surface-to-volume ratios of smaller particles in colloidal AgNP suspensions, as compared to bulk silver [28,30]. In the present study, this AgNP size-dependency was not confirmed. Despite the fact that AAS results confirmed silver release from the specimens of all size groups, the state of silver and presence of functionalization is not known. As a result, the stability and dissolution capacity of the initial AgNPs might have been differentiated. This provides a possible explanation of the absence of size-dependency in the results of the present study.

It is well-documented in the literature that AgNPs may exhibit a strong cytotoxic and genotoxic effect towards eukaryotic cells [31]. Although the underlying mechanisms of toxicity are not clear yet, it has been demonstrated that AgNPs can lead to silver ion release, leading to oxidative stress, lipid peroxidation, protein dysfunction and DNA degradation [20,32,33]. However, the induced toxicity appears to be a dose-dependent phenomenon, as exposure to low AgNP concentrations (up to 2–2.5 μg/ml) does not affect cell viability [34,35]. In the current study, the highest observed concentration of released silver at 72 h (0.39 μg/ml) was much lower than the thresholds of toxicity. The absence of dead SaOS-2 cells and the increased cell viability rates was further confirmed by confocal microphotographs, while SEM observations also indicated favorable cell attachment and morphology.

The enhanced mitochondrial activity after 24 h of incubation is in agreement with previous in vitro studies, that revealed increased cell metabolic activity measured by the MMT assay after the direct incubation with AgNPs at concentrations lower than the threshold of toxicity (<2–2.5 μg/ml) [24,35–37]. The AgNP-induced effect may be explained by their potential incorporation inside the eukaryotic cells. The major endocytic mechanisms of AgNPs have been shown to be performed through clathrin- and caveolae-mediated endocytosis [37–39]. As for the action of the AgNPs, it has been mentioned that they act as a transport vehicle to deliver silver ions into the cells. This kind of transport mechanism is called the "Trojan horse mechanism" [21,33,40].

In the present in vitro study, the increased metabolic activity of mitochondria that was observed at all the test groups compared to the control group could be the result of

an increased mitochondrial biogenesis, due to the oxidative stress known to be induced by the endocytosed silver ions [41]. The oxidative stress refers to the imbalance between the production of reactive oxygen species (ROS) and the cell's ability to detoxify and inactivate these reactive intermediates [42]. ROS include free radicals and peroxides, such as the superoxide (O_2—), hydroxyl (OH) and hydrogen peroxide (H_2O_2) [43]. Plenty of studies have shown that the excessive production of ROS provoked by AgNPs, functions as "intracellular signal" from the mitochondria to the nucleus. The nucleus receives the "signal" from the mitochondria to activate specific molecular mechanisms triggering mitochondria biogenesis to produce more energy for the synthesis of proteins and the repair of the damages caused by the ROS and the oxidative stress [41,43,44]. Indeed, in vitro studies have revealed that exposure of eukaryotic cells to oxidative stress by treatment with low concentrations of H_2O_2 leads to the increased mitochondrial metabolic activity measured by the MTT assay, as well as to the increased mitochondria number and mitochondrial DNA [41,45]. Plethora of studies have revealed that the intracellular transduction pathways that lead to mitochondrial biogenesis and activated by the oxidative stress are the P13/Akt and the AMPK pathways, both induce the synthesis of transcription factors, such as the NRF-1 and PGC-1 and the mitochondrial transcription factor mtTFA [46,47].

In addition to the MTT metabolic-based test, the BrdU assay, was employed to target another biological endpoint related to AgNP cytotoxicity on SaOS-2 cells, i.e. the cell proliferation rates. The BrdU assay allows the detection of cells, which are in the S phase of the cell cycle, as it is incorporated into newly synthesized DNA [48]. Despite the increased cell metabolic activity shown by the MTT assay, there was concentration-dependent reduction of cell proliferation rates at 48 h. This trend was present in all test groups, regardless of AgNPs size (5 or 30 nm). At 72 h, there was a recovery of the SaOS-2 proliferation rates, related to the all test groups of 5 nm AgNPs. On the contrary, this recovery did not appear in the test groups of 30 nm AgNPs.

Interestingly, cell cycle arrest seems to be a compensatory response to AgNP-induced oxidative stress [49]. Increased levels of intracellular ROS induce the expression of p21, an important inhibitor of cyclin-dependent kinases (CDK), such as CDK2, CDK4 and CDK6, which belong to the main controlling mechanisms of cell cycle progression [50]. The inhibition of CDKs leads to a transient cell cycle arrest at G1/S and G2/M checkpoints, to activate the antioxidative mechanisms and repair the damage [51]. However, severe oxidative stress can trigger irreversible cell cycle arrest and, subsequent apoptosis in a caspase-mediated pathway [52]. The last phenomenon does not apply in our study, because high cell viability was confirmed by SEM, confocal microscopy and MTT assays.

The aforementioned parallel phenomena do not indicate cell toxicity and can be explained by the cell defense mechanisms when exposed to conditions of low oxidative stress. According to various studies, AgNPs induce oxidative stress leading to the production of Reactive Oxygen Species (ROS) [53]. As a result, the eukaryotic cell reacts in two ways. Firstly, the metabolic activity is enhanced in order to supply energy to meet the need for cell survival including the repair of damage and synthesis of new proteins [41,43–47]. This is in line with the MTT results of this study showing increased metabolic activity. Secondly, the cell reduces its proliferative capacity in order to avoid the replication of the possibly damaged DNA [49]. Under low oxidative stress, cell cycle is delayed and after the damage is repaired or eliminated the cell re-enters the cell cycle and resumes to normal growth and recovery [50,51]. This is in accordance with the BrdU assay results of this study that showed delays in cell proliferation. Overall, these results warrant further investigation on the underlying mechanisms of the observed transient delay of cell proliferation in direct contact with the experimental AgNP-doped titanium surfaces.

Furthermore, at 72 h, two different patterns of SaOS-2 proliferation recovery and arrest were observed in the test groups of 5 and 30 nm AgNPs, respectively. This divergence can be attributed to differential nanoparticle kinetics of the two particle-size distribution groups. Evidence from both experimental and theoretical models suggests, that smaller nanoparticles are internalized faster into the cell, with a range of optimum radii of 25–50 nm showing the lowest wrapping times [21,54]. As already mentioned, AgNPs are internalized into the cells mainly via receptor-mediated endocytosis [55]. This two-staged thermodynamic process includes membrane invagination, to produce a favorable contact area, and nanoparticle wrapping [56]. Ligand–receptor interaction, the driving force of endocytosis, opposing to a resistance to membrane deformation during invagination, are reportedly the most critical factors during internalization process [55,56]. Consequently, there is a tendency of a slower uptake for particles larger than 50 nm, because the formation of more cell membrane receptors is required [55,57]. On the other hand, when particle radius decreases below 25 nm, the resistance to cell membrane bending becomes unfavorable [56]. As a result, wrapping time decreases and cell internalization becomes relatively slower [57].

In contrast to endocytosis, exocytosis also occurs at faster rates as nanoparticle size decreases, but without the existence of an optimal radius [58]. Consequently, when both endocytosis and exocytosis phenomena take place, particles in the range of optimal sizes accumulate intracellularly [55]. In the study of Clithrani et al., uptake and removal rates of gold nanoparticles, sized between 14 and 100 nm were investigated in various mammalian cell lines. It was demonstrated that nanoparticles around 50 nm showed the highest accumulation rates [55]. In our study, the groups of 30 nm AgNPs were related to a higher percentage of particles within the optimal radii, possibly resulting in higher intracellular accumulation rates. This phenomenon can explain the fact that proliferation rates of SaOS-2 cultures in direct contact to 30 nm AgNPs do not improve at 72 h, while there is a recovery in the groups of 5 nm AgNPs.

Regarding the antibacterial effects, CFU reduction was assessed after 24 h of direct contact with the specimens. There is a plethora of studies investigating the short-term antibacterial activity of AgNP-doped surfaces [9,13,25,36,59]. The first 6 h post-implantation have been reported to be a critical period, during which early phenomena of biofouling take place [60]. The initial 2 h phase (Phase I) is related to reversible and non-specific interactions, such as dipole–dipole and hydrogen bonding, gravitational, van der Waals, electrochemical and hydrophobic forces. Phase I is followed by

another 3 h period (Phase II), which involves specific molecular bacterial adhesion to the substrate, facilitated by polysaccharides and adhesin proteins [61]. After phase II, biofilm development and maturation lead to colonization of a more complex and heterogenous bacterial microbiota and secretion of a protective exopolysaccharide layer [61]. According to several authors, prevention of bacterial adhesion during the first post-operative 24 h, decreases the probability of biofilm growth and is vital for the long-term success of the implant [59].

In the present study, antibacterial effect was investigated on two Gram-, rod-shaped, anaerobic, periopathogenic bacteria, *P. gingivalis* and *P. intermedia*, both been associated with the evolution of periimplantitis [62]. Hultin et al., comparing microbial profile in healthy and periimplantitis sites, reported high levels of *A. actinomycetemcomitans, P. gingivalis, P. intermedia, B. forsythus and T. denticola* [63]. In their systematic review, Perez-Chaparro et al. reported that there is "moderate" and "some" evidence, respectively, to relate *P. gingivalis* and *P. intermedia* to the microbiological profile of peri-implantitis [64].

In agreement with other studies, we demonstrated a concentration-dependent reduction in colony-forming capacity of both *P. gingivalis* and *P. intermedia,* up to 30%. However, data related to the antibacterial effect of AgNPs on those two bacteria are limited. In one study, Bahador et al. developed a 25 ppm AgNP- Mineral Trioxide Aggregate Paste (NanoAg-MTA), which exhibited a 32–60% reduction *in P. intermedia* viability in a 3–48 h incubation period [65]. Both Zheng et al. and Liao et al. reported an antibacterial effect of an AgNP-doped titanium surface of more than 90% [13,66]. However, differences in deposition methodology, surface topography, silver concentration and release, nanoparticle size, shape and functionalization make direct comparisons with the present study impossible. On the other hand, data on other Gram– bacteria are comparable to this study. At AgNP concentrations comparable to the ones of this study (0.2 μg/ml), Gurunathan et al., demonstrated up to 30% antibacterial activity against the Gram- bacteria *P. aeruginosa* and *S. flexneri* [67].

Mechanisms of toxicity seem to be the same in eukaryotic and prokaryotic cells [59]. However, bacteria are more prone to AgNPs toxicity [9,65]. The difference can be attributed to the fact, that from an evolutionary perspective, bacteria are less complex cell structures [68]. For example, the lack of nuclear membrane allows their circular double-stranded DNA to be exposed to the presence of AgNPs, silver ions and ROS derivatives in their cytoplasm [69]. Simultaneously, bacteria possess simpler antioxidative and DNA-repair pathways [70]. Consequently, they are more sensitive to oxidative stress.

According to our findings, there seems to be a "therapeutic window" of AgNP-doped Ti_6Al_4V surfaces, predominantly those in which 5 and 30 nm colloidal silver dispersions were electrochemically deposited at a concentration of 300 ppm. These specimens maintain high osteoblastic cell (SaOS-2) viability and induce mild but statistically significant antibacterial activity on *P. gingivalis* and *P. intermedia* strains, which is in-line with the low AgNP concentrations detected, as well as with data found in literature [71]. These data overall fulfill the main goal of the present study in developing a "non-friendly" towards bacteria surface, while being non-cytotoxic to eukaryotic cells. Future studies both in vitro and in vivo, should be conducted to confirm these results and further investigate certain cell and bacterial gene expressions and intracellular nanoparticle kinetics.

5. Conclusions

In the current study, AgNP-doped titanium surfaces were developed using electrochemical deposition. Both eukaryotic cell biocompatibility and antibacterial effects on periopathogenic bacteria were investigated, in relation to silver release in biologic media. The test surfaces resulted in high cell viability, while the initial arrest of their proliferation rate recovered completely at 72 h. A mild antibacterial effect, up to 30%, was demonstrated against *P. gingivalis* and *P. intermedia,* two peri-implantitis associated-bacteria strains. Both excellent biocompatibility and antibacterial activity of the surfaces suggest that AgNP-doped surfaces are potential candidates for future dental and maxillofacial implant applications.

Competing interests

The authors state that they have no conflict of interest.

Acknowledgements

This research did not receive any grant from funding agencies in the public, commercial or not-for-profit sectors and was supported by Internal Departmental funding covering graduate student research. We would like to thank the companies ADIN Dental Implant Systems, Avula, Israel for providing the titanium specimens and PLiN Nanotechnology S.A., Thessaloniki, Greece for providing the silver nanoparticle stock solutions. We would also like to thank Assist Prof. Lambrini Papadopoulou, Department of Mineralogy-Petrology-Ec. Geology, School of Geology, Faculty of Sciences, A.U.Th, Greece for her assistance in the capture and interpretation of the SEM figures of SAOS-2-seeded specimens. Finally, we would also like to acknowledge the technical assistance of Mr. Boukercha and Mrs Ursula Giebel for the SEM/EDX analysis and R. Meya and K. Brauner for the AAS analysis (University of Duisburg-Essen).

REFERENCES

[1] Goodman SB, Yao Z, Keeney M, Yang F. The future of biologic coatings for orthopedic implants. Biomaterials 2013;34:3174–83.
[2] Jemt T, Johansson J. Implant treatment in the edentulous maxillae: a 15-year follow-up study on 76 consecutive patients provided with fixed prostheses. Clin Implant Dent Relat Res 2006;8:61–9.
[3] Becker W, Hujoel P, Becker BE, Wohrle P. Dental implants in an aged population: evaluation of periodontal health, bone loss, implant survival and quality of life. Clin Implant Dent Relat Res 2015;17:461–8.
[4] Faris PM, Ritter MA, Davis KE, Priscu HM. Ten-year outcome comparison of the anatomical graduated component and

vanguard total knee arthroplasty systems. J Arthroplasty 2015;30:1733–5.
[5] Subramani K, Jung RE, Molenberg A, Hammerle CHF. Biofilm on dental implants: a review of the literature. J Oral Maxillofac Implants 2009;24:616–26.
[6] Kirmanidou Y, Sidira M, Drosou ME, Bennani V, Bakopoulou A, Tsouknidas A, et al. New Ti-alloys and surface modifications to improve the mechanical properties and the biological response to orthopedic and dental implants: a review. Biomed Res Int 2016;2016:1–21.
[7] Stigter M, Bezemer J, de Groot K, Layrolle P. Incorporation of different antibiotics into carbonated hydroxyapatite coatings on titanium implant, release and antibiotic efficacy. J Control Release 2004;99:127–37.
[8] Antoci V, Adams CS, Hickok NJ, Shapiro IM, Parvizi J. Antibiotics for local delivery systems cause skeletal cell toxicity in vitro. Clin Orthop Relat Res 2007;462:200–6.
[9] Shen X, Zhang Y, Xiao F, Zhu J, Zheng X. Effects on cytotoxicity and antibacterial properties of the incorporations of silver nanoparticles into the surface coating of dental alloys. J Zhejiang Univ Sci B 2017;18:615–25.
[10] Chernousova S, Epple M. Silver as antibacterial agent: ion, nanoparticle, and metal. Angew Chem Int Ed 2013;52:1636–53.
[11] Kalishwaralal K, BarathManiKanth S, Pandian SRK, Deepak V, Gurunathan S. Silver nanoparticles impede the biofilm formation by *Pseudomonas aeruginosa* and *Staphylococcus epidermidis*. Colloid Surf B: Biointerfaces 2010;79:340–4.
[12] Besinis A, De Peralta T, Handy R. The antibacterial effects of silver, titanium dioxide and silica dioxide nanoparticles compared to the dental disinfectant chlorhexidine on *Streptococcus mutans* using a suite of bioassays. Nanotoxicology 2014;8:1–16.
[13] Zheng Y, Li J, Liu X, Sun J. Antimicrobial and osteogenic effect of Ag-implanted titanium with a nanostructured surface. Int J Nanotechnol 2012;7:875–84.
[14] Yang H, Liu C, Yang D, Zhang H, Xi Z. Comparative study of cytotoxicity, oxidative stress and genotoxicity induced by four typical nanomaterials: the role of particle size, shape and composition. J Appl Toxicol 2009;29:69–78.
[15] He P, Liu H, Li Z, Liu Y, Xu X, Li J. Electrochemical deposition of silver in room-temperature ionic liquids and its surface-enhanced Raman Scattering effect. Langmuir 2004;20:10260–7.
[16] Kar A, Raja KS, Misra M. Electrodeposition of hydroxyapatite onto nanotubular TiO_2 for implant applications. Surf Coat Technol 2006;201:3723–73.
[17] Chatzistavrou X, Fenno JC, Faulk D, Badylak S, Kasuga T, Boccaccini AR, et al. Fabrication and characterization of bioactive and antibacterial composites for dental applications. Acta Biomater 2014;10:3723–32.
[18] Yu S, Yin Y, Liu J. Silver nanoparticles in the environment. Environ Sci Process Impacts 2013;15:78–92.
[19] Xiu Z, Zhang Q, Puppala H, Colvin V, Alvarez PJ. Negligible particle-specific antibacterial activity of silver nanoparticles. Nano Lett 2012;18:4271–5.
[20] Ahlberg S, Rancan F, Epple M, Loza K, Hoppe D, Ladermann J, et al. Comparison of different methods to study effects of silver nanoparticles on the pro- and antioxidant status of human keratinocytes and fibroblasts. Methods 2016;109:55–63.
[21] Hsiao IL, Hsieh YK, Wang CF, Chen IC, Huang YJ. Trojan-Horse mechanism in the cellular uptake of silver nanoparticles verified by direct intra-and extracellular silver speciation analysis. Environ Sci Technol 2015;49:3813–21.
[22] AshaRani PV, Mun GLK, Hande P, Valiyaveettil S. Cytotoxicity and genotoxicity of silver nanoparticles in human cells. ACS Nano 2009;3:279–90.
[23] Albers CE, Hofstetter W, Siebenrock KA, Landmann R, Klenke FM. In vitro cytotoxicity of silver nanoparticles on osteoblasts at antibacterial concentrations. Nanotoxicology 2013;7:30–6.
[24] Kaczmarek M, Jurczyk K, Koper J, Paszel-Jaworska A, Romaniuk A, Lipinska N, et al. In vitro biocompatibility of anodized titanium with deposited silver nanodendrites. J Mater Sci 2016;51:5259–70.
[25] Roy M, Fielding GA, Beyenal H, Bandyopathy A, Bose S. Mechanical, in vitro antimicrobial and biological properties of plasma-sprayed silver-doped hydroxyapatite coating. ACS Appl Mater Interfaces 2012;4:1341–9.
[26] Kawahara K, Tsuruda K, Morishita M, Uchida M. Antibacterial effect of silver-zeolite on oral bacteria under anaerobic conditions. Dent Mater 2000;16:452–5.
[27] Gliga AR, Skoglund S, Wallinder I, Fadeel B, Karlsson H. Size-dependent cytotoxicity of silver nanoparticles in human lung cells: the role of cellular uptake, agglomeration and Ag release. Part Fibre Toxicol 2014;11(11).
[28] Zhang W, Yao Y, Sullivan N, Chen Y. Modeling the primary size effects of citrate-coated silver nanoparticles on their ion release kinetics. Environ Sci Technol 2011;45:4422–8.
[29] Dobias J, Bernier-Latmani R. Silver release from silver nanoparticles in natural waters. Environ Sci Technol 2013;47:4140–6.
[30] Luo W, Hu W, Xiao S. Size effect on the thermodynamic properties of silver nanoparticles. J Phys Chem C 2008;112:2359–69.
[31] Akter M, Sikder MT, Rahman MM, AKMA Ullah, Hossain KFB, Banik S, et al. A systematic review on silver nanoparticles-induced cytotoxicity: physicochemical properties and perspectives. J Adv Res 2018;9:1–16.
[32] AshaRani PV, Mun GLK, Hande MP, Valiyaveettil S. Cytotoxicity and genotoxicity of silver nanoparticle in human cells. ACS Nano 2009;3:279–90.
[33] Park EJ, Yi J, Kim Y, Choi K, Park K. Silver nanoparticles induce cytotoxicity by a Trojan-horse type mechanism. Toxicol in Vitro 2010;24:872–8.
[34] Yusuf A, Brophy A, Gorey B, Casey A. Liposomal encapsulation of silver nanoparticles enhances cytotoxicity and causes induction of reactive oxygen species independent apoptosis. J Appl Toxicol 2017;38:616–27.
[35] Kaba S, Egorova EM. In vitro studies of the toxic effect of silver nanoparticles on Hela and U937 cells. Nanotechnol Sci Appl 2015;8:19–29.
[36] Fiedler J, Kolitsch A, Kleffner B, Henke D, Stenger S, Brenner R. Copper and silver ion implantation of aluminium oxide-blasted titanium surfaces: proliferative response of osteoblasts and antibacterial effects. Int J Artif Organs 2011;34:882–8.
[37] Miranda RR, Bezerra AG, Ribeiro CA, Randi MA, Voigt CL, Skytte L, et al. Toxicological interactions of silver nanoparticles and non-essential metals in human hepatocarcinoma cell line. Toxicol in Vitro 2017;40:134–43.
[38] Milić M, Leitingerb G, Pavičića I, Avdičević M, Dobrovićd S, Goesslere W, et al. Cellular uptake and toxicity effects of silver nanoparticles in mammalian kidney cells. J Appl Toxicol 2015;35:581–92.
[39] Hsiao I, Hsieh Y, Chuang C, Wang C, Huang Y. Effects of silver nanoparticles on the interactions of neuron- and glia-like cells: toxicity, uptake mechanisms, and lysosomal tracking. Environ Toxicol 2017;32:1742–53.
[40] De Matteis V, Malavindi M, Galeone A, Brunetti V, De Luca E, Kote S, et al. Negligible particle-specific toxicity mechanism of silver nanoparticles: the role of Ag+ ion release in the cytosol. Nanomedicine 2015;11:731–9.
[41] Lee CF, Liu C, Hsieh R, Wei Y. Oxidative stress-induced depolymerization of microtubules and alteration of

mitochondrial mass in human cells. Ann N Y Acad Sci 2005;1042:246–54.
[42] Ray P, Huang B, Tsuji Y. Reactive oxygen species (ROS) homeostasis and redox regulation in cellular signaling. Cell Signal 2012;24:981–90.
[43] Marchi S, Giorgi C, Suski J, Agnoletto Bononi A, Bonora M, et al. Mitochondria-ros crosstalk in the control of cell death and aging. J Signal Transduct 2012;2012:329635.
[44] Teodoro J, Simo˜es A, Duarte F, Rolo A, Murdoch R, Hussain S, et al. Assessment of the toxicity of silver nanoparticles in vitro: a mitochondrial perspective. Toxicol in Vitro 2011;25:664–70.
[45] Chen Q, Bartholomew J, Campisi J, Acosta M, Reagan J, Ames B. Molecular analysis of H_2O_2-induced senescent-like growth arrest in normal human fibroblasts: p53 and Rb control G1 arrest but not cell replication. Biochem J 1998;15:43–50.
[46] Gugneja S, Scarpulla R. Serine phosphorylation within a concise amino-terminal domain in nuclear respiratory factor 1 enhances DNA binding. J Biol Chem 1997;30:18732–9.
[47] Irrcher I, Ljubicic V, Hood D. Interactions between ROS and AMP kinase activity in the regulation of PGC-1 transcription in skeletal muscle cells. Am J Physiol Cell Physiol 2009;1:116–23.
[48] Leif R, Stein JH, Zucker RM. A short history of the initial application of Anti-5-BrDU to the detection and measurement of S phase. Cytometry A 2004;58A:45–52.
[49] Mytych J, Zebrowski J, Lewinska A, Wnuk M. Prolonged effects of silver nanoparticles on p53/p21 pathway-mediated proliferation, DNA damage response and methylation parameters in HT22 hippocampal neuronal cells. Mol Neurobiol 2017;54:1285–300.
[50] Macip S, Igarashi M, Fang L, Chen A, Pan Z-Q, Lee SW, et al. Inhibition of p21-mediated ROS accumulation can rescue p21-induced senescence. EMBO J 2002;21:2180–8.
[51] Gauron C, Rampon C, Bouzaffour M, Ipendey E, Teillon MV, Vriz S. Sustained production of ROS triggers compensatory proliferation and is required for regeneration to proceed. Sci Rep 2013;3:2084–93.
[52] Martin KR, Barrett JC. Reactive oxygen species as double-edged swords in cellular processes: low-dose cell signaling versus high-dose toxicity. Hum Exp Toxicol 2002;21:71–5.
[53] Guo D, Zhu L, Huang Z, Zhou H, Ge Y, Ma W, et al. Anti-leukemia activity of PVP-coated silver nanoparticles via generation of reactive oxygen species and release of silver ions. Biomaterials 2013;34, 7884e7894.
[54] Zhang S, Li J, Lykotrafitis G, Bao G, Suresh S. Size-dependent endocytosis of nanoparticles. Adv Mater 2009;21:419–24.
[55] Clithrani BD, Chan WCW. Elucidating the mechanism of cellular uptake and removal of protein-coated gold nanoparticles of different sizes. Nano Lett 2007;7:1542–50.
[56] Li Y, Yue T, Yang K, Zhang X. Molecular modeling of the relationship between nanoparticle shape anisotropy and endocytosis kinetics. Biomaterials 2012;33:4965–73.
[57] Oh N, Park JH. Endocytosis and exocytosis of nanoparticles in mammalian cells. Int J Nanomed Nanosurg 2014;9(Suppl 1):51–63.
[58] Aoyama Y, Kanamori T, Nakai T, Sasaki T, Horiuchi S, Sando S, et al. Artificial viruses and their application to gene delivery. Size-controlled gene coating with glycocluster nanoparticles. J Am Chem Soc 2003;125:3455–7.
[59] Surmeneva MA, Sharonova AA, Chernousova S, Prymak O, Loza K, Tkachev MS, et al. Incorporation of silver nanoparticles into magnetron-sputtered calcium phosphate layers on titanium as an antibacterial coating. Colloids Surf B Biointerfaces 2017;156:104–13.
[60] Hentrick EM, Schoenfisch MH. Reducing implant-related infections: active release strategies. Chem Soc Rev 2006;35:780–9.
[61] Busscher HJ, Weerkamp AH. Specific and non-specific interactions in bacterial adhesion to solid substrata. FEMS Microbiol Rev 1978;46:165–73.
[62] Shibli JA, Melo L, Ferrari DS, Figueiredo LC, Faver M, Feres M. Composition of supra- and subgingival biofilm of subjects with healthy and diseased implants. Clin Oral Implants Res 2008;19:975–82.
[63] Hultin M, Gustafsson A, Hallstrom H, Johansson LA, Ekfeldt A, Klinge B. Microbiological findings and host response in patients with peri-implantitis. Clin Oral Implants Res 2002;13:349–58.
[64] Perez-Chaparro PJ, Mendes Duarte P, Shibli JA, Montenegro S, Heluy SL, Figueiredo LC, et al. The current weight of evidence of the microbiological profile associated with peri-implantitis: a systematic review. J Periodontol 2016;87:1295–304.
[65] Bahador A, Pourakbari B, Bolhari B, Hashemi F. In vitro evaluation of the antimicrobial activity of nanosilver-mineral trioxide aggregate against frequent anaerobic oral pathogens by a membrane-enclosed immersion test. Biomed J 2015;38:77–83.
[66] Liao J, Anchun M, Zhu Z, Quan Y. Antibacterial titanium plate deposited by silver nanoparticles exhibits cell compatibility. Int J Nanotechnol 2010;5:337–42.
[67] Gurunathan S, Woong Han J, Kwon D-N, Kim JH. Enhanced antibacterial and anti-biofilm activities of silver nanoparticles against Gram-negative and Gram-positive bacteria. Nanoscale Res Lett 2014;9:373–90.
[68] Erill I, Campoy S, Barbe J. Aeons of distress: an evolutionary perspective on the bacterial SOS response. FEMS Microbiol Rev 2007;31:637–56.
[69] Morita R, Nakane S, Shimada A, Inoue M, Iino H, Wakamatsu T, et al. Molecular mechanisms of the whole DNA repair system: a comparison of bacterial and eukaryotic systems. J Nucleic Acids 2010;2010:179594.
[70] Vatansever F, de Melo WCMA, Avci P, Vecchio D, Sadasivam M, Gupta A, et al. Antimicrobial strategies centered around reactive oxygen species-bactericidal antibiotics, photodynamic therapy and beyond. FEMS Microbiol Rev 2013;37:955–89.
[71] Pokrowiecki R, Zaręba T, Szaraniec B, Palka K, Menaszek E, Tyski S. In vitro studies of nanosilver-doped titanium implants for oral and maxillofacial surgery. Int J Nanomedicine 2017;12:4285–97.